COPY 2

UCRL- 1151

UNIVERSITY OF CALIFORNIA — BERKELEY

TWO-WEEK LOAN COPY

This is a Library Circulating Copy which may be borrowed for two weeks. For a personal retention copy, call Tech. Info. Division, Ext. 5545

RADIATION LABORATORY

DISCLAIMER

This document was prepared as an account of work sponsored by the United States Government. While this document is believed to contain correct information, neither the United States Government nor any agency thereof, nor the Regents of the University of California, nor any of their employees, makes any warranty, express or implied, or assumes any legal responsibility for the accuracy, completeness, or usefulness of any information, apparatus, product, or process disclosed, or represents that its use would not infringe privately owned rights. Reference herein to any specific commercial product, process, or service by its trade name, trademark, manufacturer, or otherwise, does not necessarily constitute or imply its endorsement, recommendation, or favoring by the United States Government or any agency thereof, or the Regents of the University of California. The views and opinions of authors expressed herein do not necessarily state or reflect those of the United States Government or any agency thereof or the Regents of the University of California.

UCRL-1151
Unclassified - Physics Distribution

UNIVERSITY OF CALIFORNIA

Radiation Laboratory

Contract No. W-7405-eng-48

GAMMA RAY SPECTRUM FROM THE ABSORPTION OF NEGATIVE PI MESONS IN DEUTERIUM

R. Lee Aamodt

March 1, 1951

Berkeley, California

Gamma Ray Spectrum from the Absorption of Negative Pi Mesons in Deuterium

Outline

I Introduction

II Method

A. Geometry

B. Pressure Vessel and Cooling System

C. Pair Spectrometer

D. Pumping System

E. Procedure

III Results and Conclusions

A. Competing Processes

B. The n-n Interaction

IV Acknowledgments

V Appendices

A. Mesons Stopped in Deuterium

B. Scattering

C. Radiation Straggling

D. Channel Width

E. "f" Factor

F. Selection Rules

VI References

VII Figures

I INTRODUCTION

Within two years after the postulate of Yukawa that a particle about 300 times as heavy as the electron might be responsible for nuclear forces, evidence was found that positive and negative charged particles of this order of mass were present in cosmic rays.[1][2]

Measurements on the absorption of these "mesons"* in the atmosphere and in equal amounts of condensed matter gave differences which were attributed to decay in flight, and served to measure the mean life as approximately 2 μs.[3]

At about this same time, a powerful tool for the identification of mesons and measurement of some of their properties was developed by F. Rasetti.[4] He set up a counter telescope which detected the delayed electron emitted from mesons brought to rest in an iron absorber. Using a similar system, Nereson and Rossi[5] found that approximately 1/2 of the penetrating cosmic ray particles stopped in their absorber (lead, brass, or aluminum) gave rise to delayed electrons. This was as expected, since negative mesons were assumed to be captured by the positively charged nuclei of the absorber before they could decay. Conversi, et al., made a fundamental improvement in the experimental arrangement by using magnetized iron plates to concentrate mesons of one sign in the absorber, excluding those of opposite sign.[6] They found the suprising result that negative mesons were not absorbed before decay if the absorbing material was carbon, although they were absorbed as expected in iron.

This result provided strong evidence for a fact which had been suggested by the meson half-life and earlier absorption measurements: these

---

* The discoverers called them "mesotrons" but the notation used here has apparently become established in the literature.

mesons could not be the ones postulated by Yukawa. Attempts were made to explain away the results in some other manner, but detailed study of the capture process[7] showed a discrepancy of the order of 10^{10} between experimental and theoretical capture time.

Fortunately, a heavier meson which did interact strongly with nuclei was discovered at about this same time through the study of nuclear emulsions exposed to high altitude cosmic rays.[8] These heavy mesons, designated "π" mesons, were short-lived and were formed in the upper atmosphere, so very few of them were present at sea level. Their decay product was the ordinary sea-level meson, now called the "μ" meson. The heavy negative mesons were captured in the nuclear emulsion to form "stars," many pronged energetic nuclear explosions, while the μ mesons were only rarely observed to form stars when captured.[9]

The discovery that mesons could be produced artificially[10] led to better values for the meson masses, and it was found possible to set up a consistent meson decay and capture scheme with a minimum number of particles:[11]

1. π mesons are responsible for nuclear forces. The fact that π^- mesons form stars when captured indicates that the process goes like $\pi^- + p \longrightarrow n^*$ and the energy of the meson is not taken away by a neutral particle. The π meson has integral spin.
2. The μ's from π decay have definite range, so only one other particle, which may be taken for simplicity to be a neutrino, is emitted. $\pi^{\pm} \longrightarrow n^{\pm} + \nu$
3. In free space a μ meson decays into an electron and two neutrinos. $\mu^{\pm} \longrightarrow e^{\pm} + 2\ \nu$.

4. A μ meson may be captured by a nucleus with the emission of a neutral particle, which carries away most of the energy.

$\mu^- + p \longrightarrow n + \nu$.

The μ meson has spin 1/2.

This scheme still seems valid at this writing.

An interesting experiment from the Berkeley cyclotron was the study of gamma rays of high energy from the target.[12] These indicated the formation of neutral mesons which decayed into two or more gamma rays in less than 10^{-9} sec. Study of gamma-gamma coincidences from neutral mesons created by the synchrotron beam[13] showed that the disintegration was by two gammas, so a spin 1 neutral π^0 meson is ruled out.[14]

Cosmic ray studies[15] set a limit of 5×10^{-14} sec. on the lifetime of the π^0 meson, and allowed a measurement of its mass. The experiment of Panofsky, et al., on the gamma spectrum from the absorption of π^- mesons in high pressure hydrogen[16] showed that the reactions $\pi^- + p \longrightarrow n + \gamma$ ($E_\gamma \simeq 130$ Mev); and $\pi^- + p \longrightarrow n + \pi^0 \longrightarrow n + 2\gamma$ ($E_\gamma \simeq 70$ Mev), went with almost equal probability, and a better value was set on the π^0 mass, as well as the π^- mass.

The experiment to be described in this paper was a logical extension of the hydrogen capture experiment. Three reactions seemed possible, two of them leading to observable gamma rays: (a) $\pi^- + d \longrightarrow 2n + \gamma$; (b) $\pi^- + d \longrightarrow 2n + \pi^0 \longrightarrow 2n + 2\gamma$; (c) $\pi^- + d \longrightarrow 2n$. If the last process could go it was expected that it would be the major process, and probably no gamma rays would be observed. With the expected counting rates well known from the hydrogen experiment this would still be significant.

II METHOD

A. Geometry.

The physical set-up is shown in Fig. 1. Protons circulating in the 184-inch cyclotron at 330 Mev impinge on the tungsten target parallel to its wide dimension (1/2 inch). Mesons formed in passage pass through the .040 inch thickness of the target, through the 4 gm/cm^2 walls of the stainless steel pressure vessel, some of them finally coming to rest in the deuterium gas. The density of the deuterium is 0.098 gm/cm^3 (17) at a pressure of 2700 p.s.i. and the temperature of liquid nitrogen (77 K^o). The thickness of the wall of the pressure vessel is limited by the desirability of capturing mesons of initial energy corresponding to the rising portion of the meson yield vs. meson energy curve (App. A).

Gamma rays from the deuterium are collimated inside the tank, and the target itself is screened off from the spectrometer by a copper slab on the side of the collimator. It is important that this shielding be close to the target, so that gammas produced in the target (with intensities about 100 times that of the capture gammas) are prevented from scattering into the spectrometer except through large scattering angles. The gamma rays are collimated with a lead collimator just outside the cyclotron to reduce the area of cyclotron wall near the source that is visible from the spectrometer. Final collimation is done in the 15 foot concrete shielding surrounding the cyclotron.

B. Pressure Vessel and Cooling System.

A drawing of the pressure vessel and a flow diagram of the liquid nitrogen cooling system is shown in Fig. 2. Three thermocouples are used to indicate the pressure vessel temperature and the height of liquid nitrogen

in the reservoir, and are continuously recorded. In addition, the pressure itself serves as a good indicator if failure of the cooling system occurs. Blow-out patches lead to a 47 liter evacuated cylinder in case the pressure should rise above 3500 p.s.i.

C. Pair Spectrometer.

The pair spectrometer is built in a magnet with triangular pole faces broadened at the apex, where the converter is placed, to make the field more uniform. Two rows of geiger counters are placed along the sides of the pole face, 14 counters on each side, making a total of 27 channels (Fig. 3). Two proportional counters on each side of the magnet provide a gate signal to open the geiger counter amplifiers when an electron pair through the proportional counters gives a quadruple coincidence. The doubles rates of the proportional counters on each side of the magnet are recorded and provide a measure of the slow neutron flux in the area. The doubles rates proved to be the most satisfactory monitor for intercomparison during any one set-up.

The resolving power of the spectrometer has been carefully analyzed, a process made particularly easy in the triangular arrangement of the geiger counters, since the width of the gaussian scattering curve is constant in energy (App. B). The thickness of the converter is chosen so the width of the scattering gaussian is nearly the same as the channel width (Fig. 4 and Fig. 7). Radiation straggling is calculated[18] for one of the pair under the assumption that equal numbers of electrons arise in each equal increment of converter thickness. The resultant curve is fitted by a mathematical expression, and the effect of the straggling on the measured energy of the pair calculated (App. C), (Fig. 5). The resolving power curve for a single channel is known (App. D) to be a triangle, of base

width equal to two channel units (Fig. 4). The resolution of the spectrometer is now calculated by "folding" together the various curves representing scattering, radiation straggling and channel width, to give the final resolving power curve shown in Fig. 8. This is the shape of the experimental curve which would be obtained from a spectral line, and a check with the hydrogen spectrum at high energy confirms the theoretical curve (Fig. 9).

An additional correction is made for the spectrometer sensitivity at various energies, as determined by the number of channels available for pairs in the various regions. The assumption is made that any division of energy between the members of a pair is equally probable. The cross section for pair production is included in this "f" factor (App. E).

An electronic block diagram is shown in Fig. 10, which also shows the recording system. Data is recorded by sparks on a special paper from a row of "pens," stiff wires connected to the output of the individual geiger tubes. When a gate signal opens the geiger amplifiers, the two tubes, on opposite sides, through which the electron and positron have passed, give pulses resulting in two black dots burned in the paper below the "pens" corresponding to those channels.

D. Pumping System.

The deuterium pumping system is shown in Fig. 2 and Fig. 20. Since the deuterium must be recovered after each run it is necessary to exhaust the pressure tank to not more than one or two atmospheres in a reasonably short time. Operating pressure is 2700 p.s.i. and commercial deuterium comes at 1,000 p.s.i. This wide range of pressures must be handled in as short a time as possible, so a system of two pumps was used. A large volume (12 liter) 2,000 p.s.i. maximum pressure oil piston was made up from

standard compressed gas cylinders to complement the one liter high pressure (6500 p.s.i.) pump used on hydrogen. The final system will fill the 600 cubic centimeter pressure vessel to 2700 p.s.i. at liquid nitrogen temperature in about 30 minutes, and pump the gas down to one atmosphere gauge pressure in the same time. The oil used in the pumps is ordinary diffusion pump oil, chosen for its low vapor pressure. The purity of the deuterium gas, after standing for 48 hours over the oil at 2,000 p.s.i. was measured at 99.75 percent by a mass spectrograph analysis, indicating that hydrogen exchange between dissolved gas and the oil molecules was negligible.

E. Procedure

Before a run the collimators are aligned using a telescope sighted on the pressure vessel. At the beginning of a run the probe is run out to a larger radius, and the high intensity gamma rays from the target are used to test the equipment and run plateaus on proportional counter voltages and discriminator settings. The target is then run in and a short run made on hydrogen to determine that operation is normal and the system free from leaks before introducing the deuterium. A background run, followed by a deuterium run and a second background run takes up the remainder of a 16 hour period. The background rate is approximately one pair per minute. The rate with deuterium gas in the vessel is about 1.6 pairs per minute, and with hydrogen, about 2.0 pairs per minute with the spectrometer centered at 130 Mev. The final spectrum, involving about forty hours of running time on deuterium and twenty hours of background time, is shown in Fig. 11.

The ratio of the yield in deuterium to that in hydrogen was measured with geometry unchanged. The hydrogen yield of "low energy" gammas near

70 Mev was measured simultaneously with the yield at 130 Mev by centering the spectrometer at 100 Mev for one run (Fig. 12). From the total area under the deuterium curve and that under the hydrogen curve with the spectrometer set at 130 Mev, and with the known ratio of hydrogen "high" to "low" energy gammas, the yield from the deuterium was found to be 0.30 ± 0.05 of that in hydrogen. (No gamma rays were observed in deuterium near 70 Mev. The observed yield of "low energy" gammas from hydrogen was divided by 2 to obtain the corresponding number of π^0 emissions.) Table I gives the observed data.

It was necessary to check that the gamma rays from deuterium were not arising from protons scattered from the target and striking the neutrons in the deuterium, where they could create neutral mesons directly. A run with helium should give twice as many gammas from this source, and actually gave a null result within statistical and monitor fluctuations. A limit of 10 percent of the hydrogen effect was placed on the possible gamma emission from helium. The fact that the "background" from scattered protons is essentially a "low energy" effect, peaking around 70 Mev and going to zero at 130 Mev, while the deuterium gammas are concentrated near 130 Mev and give a null effect at 70 Mev is further evidence that the background from scattered protons in the deuterium is small.

Part of the process of capture of the π^- meson in the K shell involves the motion of the π^--μ^+ system as a whole with random thermal energies.[10] This could conceivably result in a lengthening of capture time in deuterium, the molecules moving with 0.7 of the velocity of the hydrogen molecules. To test this possibility, the rate of collisions of the hydrogen molecules was cut down by reducing the density by a factor of two. It was found that the gamma ray yield went down only by the same factor, indicating that π-μ

decay was not seriously competing with capture, and was not a possible explanation for the smaller yield of gamma rays in deuterium. (Table II)

III RESULTS AND CONCLUSIONS

A. Competing Processes.

The main experimental result of immediate theoretical interest is the inferred competition of the $\pi^- + d \longrightarrow 2n$ process with the radiative capture. If the meson is captured by the nucleus from a K orbit then it cannot be a scalar particle. (Table III). Brueckner, Serber, and Watson have shown[19] that the transition time for radiation to the ground state from p orbits is at least 30 times smaller than the transition time for the two neutron process, unless the meson nuclear interaction is so strong as to radically change the form of the p wave function near the nucleus.

Calculations with detailed meson theories[20] indicate that the observed ratio of radiative to fast neutron captures rules out both the scalar and vector π^- meson, in agreement with experimental observations of the angular distribution of photo-mesons.[21][22]

The absence of the π^0 is not of theoretical importance. The $\pi^- - \pi^0$ mass difference is 5.4 ± 1 Mev.[16] The kinetic energy available in the final state in the process $\pi^- + d \longrightarrow 2n + \pi^0$ is approximately 1.9 ± 1.0 Mev. A shift of two probable errors in the measured value would make the process impossible. In addition, the π^0 certainly does not have spin one. If the π^- and π^0 both have spin zero, either the π^0 or the two neutrons must be in the p state. This is unlikely because of the low energy available.

B. The n-n Interaction.

The shape of the deuterium spectrum, and in particular the location of the peak on an energy scale in relation to the hydrogen peak is also of theoretical interest. As has been pointed out,[20][23] the gamma ray spectrum from capture in deuterium is sensitive to the interaction of the

neutrons in the final state. Watson and Stuart[24] have calculated theoretical spectra for various values of the "binding energy" of the hypothetical di-neutron,[25][26] including virtual values, (the phase shift δ is the actual parameter to which the spectrum is related, but since the binding energy is not sensitive to choice of the radius of the n-n interaction it has been calculated on the basis of a radius the same as that for p-p forces--2.65×10^{-13} cm).

The theoretical spectra are folded* into the resolving power curve of the spectrometer, and plotted on semi-log paper for convenience of normalization in the comparison with experimental values. (Fig. 13) The resolving power curve is so broad that it makes the shape of all the resulting curves very similar. Only the position of the peak varies appreciably from one curve to the next. The shifts of the peak are not great enough, in view of the resolving power half width of 14 Mev, to allow a measurement of the "binding energy" of the two neutrons. However, to see what information might reasonably be derived from the data the following analysis was made:

1. The energy scale of the spectrometer is well known. The geometry is accurate to 1/64 inch in 20 inches, or 0.08 percent. The magnetic field, monitored by a proton moment apparatus, is known to 10 gauss in 9,000, or 0.1 percent.
2. Since the shape of the curves for various binding energies is obscured by the poor resolution, the position of the curve on the energy scale is used for analysis.
3. The position of the theoretical curves is uncertain by the uncertainty in the π^- mass value used. The position

---

* The fold h(t) of two curves f(x) and g(x) is defined to be $\int_{-\infty}^{\infty} f(x)g(x-t)dx$.

relative to the hydrogen spectrum position is constant, however, so only the uncertainty in the position of the hydrogen spectrum on the energy scale due to the fitting of the experimental data enters here. This was taken as 1 Mev[16] (Fig. 9).

4. The displacement of the theoretical curves from the curve for $E_B = 0$ is plotted in Fig. 14 as a function of E_B.

5. The experimental points are visually fitted to the curve $E_B=0$, and the displacement of the experimental energy scale from the $E_B=0$ energy scale, as estimated by four different observers is also plotted on Fig. 14, together with their estimates of the probable error combined with the 1 Mev probable error mentioned in 3.

6. Unfortunately, the resolving power of the spectrometer is not good enough to rule out the no-interaction or "plane wave" curve. This means that no conclusion can be drawn about the n-n interaction unless it is assumed that the final neutron state is a singlet S state, where the two neutrons are close enough together so their interaction can affect the spectrum. If this is assumed, a limit on the binding energy of the two neutrons of 200 Kev (real) may reasonably be placed. The assumption that the final state is singlet means that one of the nucleons has flipped over from the initial triplet state. Such behavior is consistent with the other experimental evidence that the π^- meson is not scalar.

It is evidently desirable to repeat this experiment with better resolving power when it is attainable.

IV ACKNOWLEDGMENTS

The author wishes to express his appreciation to Dr. W. K. H. Panofsky for his invaluable assistance at all stages of the experiment, including the suggestion that it be performed. His analysis of the pair spectrometer resolving power was of great assistance in writing the appendices herein, and the experimental set-up was largely the same as that which he designed for the hydrogen capture experiments.

Mr. James Hadley gave much helpful assistance with the runs, and provided the multi-channel geiger pulse amplifier and recorder, greatly facilitating the experiment.

Mr. Robert Phillips has been of great help in every run, and sincere thanks go to him, to Mr. Kenneth Crowe, and to the many others who volunteered their help during the necessarily somewhat tedious data-taking runs.

Messrs. Stripeika and Barrere spent many extra hours keeping the electronics in operation, and appreciative thanks are extended to them and to the cyclotron crew for their help.

The analysis of the n-n interaction was made possible through the theoretical work of Dr. K. Watson and Mr. R. Stuart, and the author is grateful to them for discussion of the problem and calculation of the theoretical spectra.

Gas	Approximate Energy	Process	Counts/Minute
H_2	70 Mev	$\pi^0 \longrightarrow 2\gamma$	.90 ± .18 (divide by 2)
	130 Mev	$\pi^- + p \longrightarrow n + \gamma$	.470 ± .046
			.92 ± .10 Total captures counted per minute
D_2	70 Mev	$\pi^0 \longrightarrow 2\gamma$	-.007 ± .020
	130 Mev	$\pi^- + d \longrightarrow 2n + \gamma$	.275 ± .034
			.275 ± .04 Total captures counted per minute

ratio $\dfrac{\text{captures in } D_2}{\text{captures in } H_2} = 0.30 \pm 0.05$

Table I

Tabulation of total counting rates of spectrometer with H_2 and D_2 in pressure vessel under identical conditions of geometry and incident meson flux.

Recorder	Intensity in counts/minute		
	2700 psi	1300 psi	Ratio
Number gates recorded	.853 ± .033	.523 ± .042	1.63 ± .14
Number high energy gamma rays recorded	.213 ± .013	.121 ± .017	1.74 ± .27
Density of H_2	.046	.028	1.65

Table II

Relative intensities of gamma rays at two H_2 pressures. Background has been subtracted.

Scalar π^-			d		$\pi^- - d$ system		2n		Total angular momentum	Parity	Remarks
Spin	Orbital angular momentum	Parity	Spin	Parity	Angular momentum	Parity	Spin	Orbital angular momentum			
0	0 (s state)	+	1	+	1	+	0	0(s)	0	+	NG
							1	1(p)	0,1,2	-	NG
0	1 (p state)	-	1	+	0,1,2	-	0	0	0	+	NG
							1	1	0,1,2	-	OK

Table III

Tabulation of possible combinations of parity and spin for a scalar meson where the final state is the two neutron system. Only in the case of capture from a p state can the conservation rules for parity and angular momentum be simultaneously satisfied. For further explanation see Appendix F.

V APPENDICES

A. Discussion of the variation in the number of mesons stopped in deuterium as a function of wall thickness of the pressure vessel.

B. Effect of scattering of the electron pair on the spectrometer characteristics.

C. Effect of radiation straggling of the electron pair on the measured energy of the pair.

D. The resolving power of the spectrometer due to finite channel width.

E. Calculation of the "f" factor, which is multiplied into measured gamma ray intensity to give actual intensity.

F. Explanation of Table III. Selection rules.

APPENDICES

A. Mesons Stopped in Deuterium

Let the curve giving number of mesons per unit energy of the mesons be a rising straight line, $\rho = kE$, and let the thickness of deuterium in the vessel (in equivalent grams per square cm of wall) be ΔR, a constant small compared to the vessel wall thickness, R. Those mesons whose ranges lie between R and $R + \Delta R$ will be stopped in the deuterium. The width of the energy region from which they come is $\Delta E = \left(\frac{dE}{dR}\right)_E \Delta R$. Now $\left(\frac{dE}{dR}\right)_E$ goes approximately as K/E, so $\rho \Delta E$ = number of mesons stopped in the deuterium $\simeq (kEK/E)\Delta R = kK\Delta R$, a constant. The number of mesons stopped does not change appreciably as long as we are on the more or less straight rising part of the yield curve, regardless of ρ.

B. Scattering

The triangular geometry simplifies the calculation of two quantities dependent on scattering of the electron pair in the γ-ray converter. (a) is the fraction of the electrons lost by striking the pole faces (vertical scattering). (b) is the r.m.s. width $\langle E \rangle$ of the Gaussian curve giving the probability of an electron of energy E arriving at a point corresponding to $E + \Delta E$ because of horizontal scattering.

The symbols E = energy of an electron and ρ = its radius of curvature will be used interchangeably. Let $\langle \theta \rangle_{\rho, t}$ indicate the r.m.s. plane projected scattering angle for en electron of energy ρ passing through a thickness t of scatterer. The basic formula to be used is $\langle \theta \rangle^2_{\rho, t} = \text{const.}\ t/\rho^2$.[27]

(a) Consider the magnetic field fixed. The path length followed by an electron is $\rho \phi$, where ϕ is the apex angle of the pole face.

(Fig. 15) In a distance $\rho\phi$ the electron rises $\rho\phi \sin\theta \simeq \rho\phi\,\theta$, where θ is the plane projected vertical scattering angle. If 2d is the separation of the pole pieces the average electron can rise d before striking the pole face. Now $\langle\theta\rangle \sim 1/\rho$ so $\rho\langle\theta\rangle$ is approximately constant for high energy electrons, and a constant fraction of the electrons are lost at all energies.

(b) An electron of radius ρ, scattered horizontally so that it leaves the converter at an angle θ with respect to the forward direction, arrives at the same point in the detector as an electron of radius $\rho + \Delta\rho$ which was not scattered. $\Delta\rho$ depends on ρ, θ, and the apex angle of the spectrometer, ϕ. As seen in Fig. 15, $\Delta\rho = \rho\,\theta \cot\frac{\phi}{2}$. In the present experiment $\phi = \pi/2$ and $\Delta\rho = \rho\,\theta$. (1)

The r.m.s. plane projected scattering angle $\langle\theta\rangle$ for an electron of energy ρ passing through thickness t of material may be written

$$\langle\theta\rangle = \frac{a\sqrt{t}}{\rho} \tag{2}$$

The distribution of deflections is Gaussian;

$$P(\theta) = \frac{1}{\sqrt{2\pi}\,\langle\theta\rangle}\, e^{-\frac{\theta^2}{2\langle\theta\rangle^2}} . \tag{3}$$

or $P(\theta) = \dfrac{\rho}{\sqrt{2\pi}\,a\sqrt{t}}\, e^{-\frac{\theta^2}{(2a^2t)/\rho}}$ from (2).

$P(\theta)$ may be written

$$\frac{1}{\sqrt{2\pi}\,a\sqrt{t}}\, e^{-\frac{(\rho\theta)^2}{2a^2t}}\, d(\rho\theta) = P(\rho\theta)d(\rho\theta) = P(\Delta\rho)d(\Delta\rho) \tag{4}$$

$P(\Delta\rho)$ is independent of ρ in this geometry, as mentioned previously.

For an electron pair the probability of scattering for each of the electrons is independent, so the r.m.s. deviation in the measured energy, $\rho_1 + \rho_2$, is $\sqrt{2}\,\langle\Delta\rho\rangle = \sqrt{2}\,a\sqrt{t}$. Let $\sqrt{2}\,a = a_1$. Then the

probability of a deviation $\Delta\rho$ in the measured gamma ray energy because of scattering is

$$P(\Delta\rho) = \frac{1}{\sqrt{2\pi}\,\alpha_1\sqrt{t}}\; e^{-\frac{(\Delta\rho)^2}{2\alpha_1^2 t}} \tag{5}$$

This probability may be averaged over the converter, under the assumption that equal numbers of pairs are formed in each equal increment of thickness of converter, giving the total probability for the observed energy deviations for a converter of thickness T :

$$P(\Delta\rho) = \frac{1}{\sqrt{2\pi}}\;\frac{1}{\alpha_1}\int_0^T \frac{1}{\sqrt{t}}\; e^{-\frac{(\Delta\rho)^2}{2\alpha_1^2 t}}\;\frac{dt}{T} \tag{6}$$

Let $\frac{2\,\alpha_1^2\,t}{(\Delta\rho)^2} = v^2$, and the last equation becomes

$$P(\Delta\rho) = \frac{1}{T}\;\frac{1}{\sqrt{\pi}}\;\frac{1}{\alpha_1}\;\frac{\Delta\rho}{\alpha_1}\int_0^{\frac{\alpha_1}{\Delta\rho}\sqrt{2T}} e^{-1/v^2}\;dv \tag{7}$$

$\int_0^v e^{-1/v^2}\,dv = f(v)$ may be integrated numerically. The result of such an integration is shown in Fig. 16.

$$\text{Now}\quad E = k\rho\ ,\ \text{so}\ \langle\theta\rangle = \frac{k\alpha\sqrt{t}}{E} \tag{8}$$

$$\text{Define}\ \sqrt{2}\,k\alpha = \alpha_2,\ \text{then}\ E/\alpha_2 = \frac{\rho}{\sqrt{2}\,\alpha} = \rho/\alpha_1\ . \tag{9}$$

(7) may be written

$$P(\Delta\rho)d\Delta\rho = \frac{1}{\sqrt{\pi}}\frac{1}{T}\frac{\Delta\rho}{\alpha_1}\; f\left(\frac{\sqrt{2T}}{(\Delta\rho)/\alpha_1}\right)d\left(\frac{\Delta\rho}{\alpha_1}\right) = \frac{2}{\sqrt{\pi}}\;\frac{\Delta E}{\sqrt{2T}\,\alpha_2}\; f\left(\frac{\sqrt{2T}}{(\Delta E)/\alpha_2}\right)d\,\frac{\Delta E}{\sqrt{2T}\alpha_2} \tag{10}$$

Let $\frac{\Delta E}{\sqrt{2T}\,\alpha_2} = x$. A plot of (10) in the form $P(x) = 2/\sqrt{\pi}\;\; x\, f(1/x)$ is shown in Fig. 17.

To use this universal curve, assume an electron of arbitrary energy E_1 passes through a converter of thickness T. Determine $\langle\theta\rangle$ for this electron. Then $2E_1\langle\theta\rangle = a_2\sqrt{2T}$ and $P(\Delta E) = \frac{1}{a_2\sqrt{2T}}P\left(\frac{\Delta E}{a_2\sqrt{2T}}\right)$. A plot of $P(\Delta E)$ for a 0.020 inch Ta converter is shown in Fig. 7.

C. Radiation Straggling

Heitler[12] gives the probability $w(y)dy$ that the energy of an electron has decreased to e^{-y} of its initial value in passing through a thickness t of material. The function $W(p)dp$, giving the probability that an electron from the gamma ray converter will retain a fraction between p and p + dp of its initial energy, may be generated by changing the variable from y to p and averaging over the thickness of the converter. Each of the curves $w(y)$ for various thicknesses of converter has a form like $A/y^{1-\alpha}$ where α is small, and the final averaged curve can be fitted by an expression of the form $K/(1-p)^{1-\alpha}$. Note that $p = E/E_0$, $dp = dE/E_0$. $E = e^{-y}E_0 \simeq (1-y)E_0$ for small y, so $1-y \simeq E/E_0 = p$, and $dy \simeq -dp$ to 1st order in y, so it is reasonable that such a curve would give a good fit to the actual $W(p)$ curve obtained by the averaging process, at least, if the converter is not too thick.

Besides $W(p)$, there is a function $P(E_1,E_\gamma)dE_1$, giving the probability that a pair member have an energy between E_1 and $E_1 + dE_1$ for a total pair energy E_γ. Making the assumption that any division of pair energy is equally probable, as is approximately the case, $P(E_1,E_\gamma)dE = \frac{dE_1}{E_\gamma}$.

Let the maximum energy of a pair member accepted by the spectrometer be E_B, and the minimum, E_A. Let f be defined by the expression $f = \frac{p_1E_1 + p_2E_2}{E_\gamma}$, thus f is the fraction of the initial energy measured

by the spectrometer (in the absence of other perturbing factors such as scattering and finite channel width which are treated separately).

The function which enters into the resolving power curve is $\pi(f)df$, the probability that a pair retains a fraction between f and f+ df of its initial energy. It can be derived as follows:

The probability that the energy division is E_1 and E_2 and that the pair members retain a fraction p_1 and p_2 of their initial energies such that f has values in the region df is $\pi(f)df = \iint W(p_1)dp_1 W(p_2)dp_2 P(E_1, E_\gamma)dE_1$. This is to be integrated over a region of E_1, p_1, p_2 space subject to the limits E_A, E_B on E_1; 0 and 1 on p_1 and p_2; and the relations

$$f = \frac{p_1E_1 + p_2E_2}{E_\gamma} \qquad \text{and } E_1 + E_2 = E_\gamma \ .$$

For convenience the variables are changed to p_1, f and E_1 using the relations above and the Jacobian transformation of the volume element

$$dp_1 dp_2 dE_1 \longrightarrow J\frac{(p_1 p_2 E_1)}{(p_1 f\ E_1)} dp_1 df dE_1 \ .$$

$$\pi(f)df = \int_{E_A}^{E_B} dE_1 \int_{1-\frac{E_\gamma}{E_1}(1-f)}^{1} W(p_1)W\left(\frac{E_\gamma f - p_1E_1}{E_\gamma - E_1}\right) \frac{1}{E_\gamma - E_1} \ dp_1 df \ ,$$

where the integration is over dE_1 and dp_1. The effective lower limit on p_1 is given by the requirement that $p_2 = \frac{E_\gamma f - p_1E_1}{E_\gamma - E_1}$ must be equal to or less than 1, i.e., $p_1 > 1 - \frac{E_\gamma}{E_1}(1 - f)$.

For the particular case of a 0.020 inch Ta converter it was found that $W(p) = \frac{K}{(1 - p)^{1-\alpha}}$ where $\alpha = 0.08$. No effort was made to normalize the resolving power curve since it was fitted to the experimental data plotted on semi-log paper, so K is arbitrary. After integrating, $\pi(f)$

was found to be $\dfrac{K}{(1-f)^{1-2\alpha}}$, $f < 1$

0 , $f > 1$

or $P(E) = \dfrac{1}{(E_\gamma - E)^{1-2\alpha}}$ for $E < E_\gamma$ (Fig. 5)

0 for $E > E_\gamma$.

This turns out to be, for a converter as thin as 0.02 inches Ta at least, the same straggling as would be experienced by an electron of energy E_γ passing through the full thickness of the converter.

D. Channel Width

Consider a gamma ray of energy E_γ, and the two electrons of energy E_1 and E_2 to which it gives rise. Assume equal probability for any division of the pair energies. Represent E_γ by a line OE_γ, E_1 by OE_1 and E_2 by E_1E_γ. Divide OE_γ into N_γ equal increments ΔE_γ. OE_1 may equally probably end and E_1E_γ begin in any of them. If a pair spectrometer accepts E_1 from N of these energy intervals (and it must accept both members of the pair), the measured intensity at the energy E_γ must be multiplied by a factor N_γ/N to represent the true spectrum. A convenient way to derive this correction value is as follows (Fig. 18):

Plot the radius of curvature of one electron along the x axis and the other along the y axis. Let ρ_{1A} , ρ_{1B} respectively be the limits of the spectrometer aperture on side 1, and similarly for ρ_{2A} and ρ_{2B} on side 2. (ρ_{1A}, ρ_{1B}), (ρ_{1A}, ρ_{2B}) etc. represent the 4 corners of a rectangle. Lines of slope +1 are lines $\rho_2 - \rho_1 =$ constant. Lines of slope -1 are lines $\rho_1 + \rho_2 =$ constant. For each energy $\rho_1 + \rho_2 = \rho_\gamma$, there is a line on the graph, and some of these lines pass through the rectangle. These are the energies accepted by the spectrometer, and the number of squares passed through

inside the rectangle is the number N. $\Delta\rho$ is determined by the fineness of the graph paper, and in the limit N will rise along a straight line to a maximum, descending immediately on the other side to form a triangle if the rectangle is a square. If ρ_γ varies appreciably over the rectangle this must be taken into account by dividing N by $N_\gamma = \frac{\rho_\gamma}{\Delta\rho}$. Fig. 4 shows the finite resolving power of the pair spectrometer due to finite geiger counter width. The aperture considered is one tube on each side, i.e., one "channel."

E. "f" Factor

In addition to the resolving power of the spectrometer due to finite channel width, a correction must be made for the variation of sensitivity of the spectrometer over a wide region of energy from ρ_{min} to ρ_{max}, approximately 3 to 1 in this spectrometer. This correction, the "f" factor, is arrived at as in Appendix D, with the exception that ΔE is now fixed by the finite width of the geiger tubes themselves, and the correction for the variation in ρ_γ must be made. In addition, σ, the cross section for pair production at each energy, is divided into the quantity N_γ/N to correct for the variation in cross section. Thus $f = N_\gamma/N_\sigma$, usually normalized to 1 at the sensitivity peak. This quantity (Fig. 19) is multiplied into the observed spectrum to get the true gamma ray spectrum. ρ_γ may conveniently be expressed in Mev/kilogauss as in the figure.

F. Explanation of Table III. Selection Rules.

1. Parity

Consider a system of n particles, at $r_1, r_2, \ldots\ldots, r_n$. It can be shown[28] that any physically important eigenfunction of the system has

the property that $\psi(r_1, r_2 \ldots\ldots r_n) = \pm \psi(-r_1, -r_2, \ldots\ldots -r_n)$. (1)
(Note that only the space coordinates are reflected in the origin, parity is not concerned with spin.) A state may be said to have positive or negative parity in accordance with the sign in (1).

In the calculation of the probability of a transition between states the matrix element for the transition enters. This is defined as $|H_{12}| = \int \psi_2^* H' \psi_1 \, d\tau$ (2)

where H' is the Hamiltonian operator of the perturbation causing the transition, and in general will be unaffected by a reflection in the origin. If $|H_{12}|$ is zero the direct transition is forbidden. Let

$$\psi_2^* H' \psi_1 = \phi(r_i) \tag{3}$$

$$\phi(-r_i) = \pm \psi_2^* H' (\pm \psi_1) = \pm \phi(r_i) \tag{4}$$

$\phi(r_i)$ has definite parity properties, the product of the parities of the initial and final state. Now $|H_{12}| = \int \phi(r_i) d\tau =$
$\int \phi(r_i) r_1^2 d\Omega_1 dr_1 r_2^2 d\Omega_2 dr_2 \ldots\ldots$

Integrate first over the solid angles $d\Omega_i$.

$$\int_{\Omega_i} \phi(r_i) d\tau = \int_{\Omega_i/2} \left[\phi(r_i) + \phi(-r_i)\right] d\tau \tag{5}$$

The expression on the right is obtained by integrating twice over a hemisphere instead of once over a sphere, replacing r_i by $-r_i$ for the second integration. $\phi(r_i)$ must have positive parity or the integrand will vanish. Thus the selection rule is obtained:

1. The initial and final state must have the same parity in order that a transition may occur.

In addition to this selection rule there is the conservation of

angular momentum rules:

2. The initial and final states must have the same total angular momentum, in order that a transition may occur.

In writing the rules in this way it is required that all wave functions involved be considered in each state, i.e., the gamma ray in gamma emission may take off a certain angular momentum and have odd parity, leaving behind a system of particles with different angular momentum and parity than the initial system. The total parity of the whole system is the product of the parities of its parts, if they may be described by separate wave functions and therefore be said to have a definite parity.

In Table III, the initial state is a meson in a Bohr orbit about a deuteron. The interaction of the two nucleons in the deuteron is not considered to involve the coordinates of the meson, and similarly only the center of mass of the deuteron is involved in the meson wave function, so the wave function for the initial state may be written as the product of two wave functions--the hydrogenlike wave function of the meson-deuteron system ψ_M multiplied into the deuteron wave function, ψ_d.

The deuteron wave function is mostly S wave, and its spin is 1. An S wave function only involves r, and therefore has even parity. A P wave function has odd parity, a D even, etc., as may be seen by examining the corresponding spherical harmonics. The above rules are for particles possessing what may be defined as positive "intrinsic parity," i.e., like nucleons. Certain types of particles obey the opposite rule, i.e., the so-called "pseudoscalar" and "vector" particles, and may be defined to have negative "intrinsic parity." A particle which in a K orbit about

a nucleon forms a system with the opposite parity from that of a deuteron, for example, is said to have negative intrinsic parity.

With the understanding that "scalar" and "pseudovector" types of particles have positive intrinsic parity, Table III may be understood as follows:

Case 1. The meson is in an S orbit about the deuteron. ψ_M therefore has positive parity and zero angular momentum. ψ_d has positive parity and one unit of spin. Then the initial state $\psi_M \psi_d$ has positive parity and one unit of total angular momentum. In the final state, the two neutron wave function, ψ_n, may represent a singlet S state with zero angular momentum and positive parity or a triplet P state with zero, one, or two units of angular momentum and negative parity. (The exclusion principle allows only singlet S, triplet P, singlet D, etc.) The singlet S final state does not conserve momentum. The triplet P final state does not conserve parity.

Case 2. The meson is in a P orbit about the deuteron. ψ_M has negative parity and one unit of angular momentum. ψ_d, as before, has positive parity and one unit of spin. The initial state $\psi_M \psi_d$ has negative parity and zero, one, or two units of total angular momentum. The final states are the same as in Case 1, and the transition to the triplet P state of the two neutron system is permitted.

VI REFERENCES

(1) Neddermeyer and Anderson, Phys. Rev. 51, 884 (1937)

(2) Street and Stevenson, Phys. Rev. 51, 1005 (1937)

(3) B. Rossi and D. Hall, Phys. Rev. 59, 223 (1941)

(4) F. Rasetti, Phys. Rev. 59, 706 (1941)

(5) Nereson and Rossi, Phys. Rev. 64, 199 (1943)

(6) M. Conversi, E. Pancini, O. Piccioni, Phys. Rev. 71, 209 (1947)

(7) E. Fermi and E. Teller, Phys. Rev. 72, 399 (1947)

(8) C. M. G. Lattes, H. Muirhead, G. P. S. Occhialini, C. F. Powell, Nature 159, 694 (1947)

(9) George and Trent, Nature 164, 838 (1949)

(10) E. M. Gardner and C. M. G. Lattes, Science 107, 270 (1948)

(11) R. Serber, Phys. Rev. 75, 1459 (1949)

(12) Bjorklund, Crandall, Moyer and York, Phys. Rev. 77, 213 (1950)

(13) J. Steinberger, W. Panofsky and J. Steller, Phys. Rev. 78, 802 (1950)

(14) See, e.g., C. N. Yang, Phys. Rev. 77, 243 (1950)

(15) A. Carlson, J. Hooper, and D. King, Phil. Mag. 41, 701 (1950)

(16) Panofsky, Aamodt and Hadley, Phys. Rev. (to be published)

(17) Johnson, Bezman, Rubin, Johnson, Corak, Rifkin, MDDC-850

(18) Heitler, Quantum Theory of Radiation, Oxford, 1944, p. 223 ff.

(19) Brueckner, Serber, and Watson, Phys. Rev. (to be published)

(20) S. Tamor and R. Marshak, Phys. Rev. 80, 766 (1950)

(21) Bishop, Steinberger, and Cook, Phys. Rev. 80, 291(L) (1950)

(22) K. A. Brueckner, Phys. Rev. 79, 641 (1950)

(23) S. Tamor, Thesis, University of Rochester, 1950

(24) K. M. Watson and R. N. Stuart, UCRL-1086 and Bull. Am. Phys. Soc. 26, 23 (1951) (New York Meeting)

(25) N. Feather, Nature 162, 213 (1948)

(26) Allen, Almqvist, Dewan and Pepper, Bull. Am. Phys. Soc. 25, 27 (1950)

(27) Rossi and Greisen, Rev. Mod. Phys. 13, 249 (1941)

(28) See, e.g., Fermi (Compiled by Orear, Rosenfeld, and Schluter) Nuclear Physics, University of Chicago (1950), p. 98.

VII FIGURES

1. Geometrical arrangement of apparatus.

2. Flow diagram of liquid N_2 and gaseous D_2 system, with detail of pressure vessel.

3. Pole face of spectrometer magnet, showing geiger counter and double proportional counter arrangement.

4. Expected distribution of measured energy values because of finite channel width.

5. Expected distribution of measured energy values because of radiation straggling of electrons.

6. Expected distribution of measured energy values because of finite channel width and radiation straggling combined.

7. Expected distribution of measured energy values because of scattering of electrons.

8. Expected distribution of measured energy values because of finite channel width, radiation straggling, and scattering of electrons, combined.

9. Comparison of theoretical distribution of measured energy values with experimental points from the hydrogen mono-energetic gamma ray, plotted on semi-logarithmic paper.

10. Block diagram of electronics.

11. Final deuterium spectrum.

12. Hydrogen run from which ratio of "high" to "low" energy gamma rays was measured.

13. Theoretical deuterium spectra for various n-n binding energies, "folded" into the resolving power curve of the spectrometer and plotted on semi-logarithmic paper, with the experimental points.

14. Displacement of theoretical curves from "$E_B = 0$" curve, plotted against E_B. The four points with probable errors are the values estimated by four observers by visually fitting the experimental points to the "$E_B = 0$" curve.

15. Geometry used to estimate the measured energy of scattered electrons as a function of the apex angle of the pole face and the scattering angle. For the 90° apex angle used, $\Delta\rho = \rho\theta$ (App. B).

16. The function $f(v)$ (App. B).

17. Universal scattering curve P(x). For explanation see App. B.

18. Lattice used to calculate resolving power of spectrometer with arbitrary apertures on each side. Equal apertures give triangular resolving power as shown in Fig. 4.

19. The "f" factor curve (App. E).

20. The high pressure pumping system.

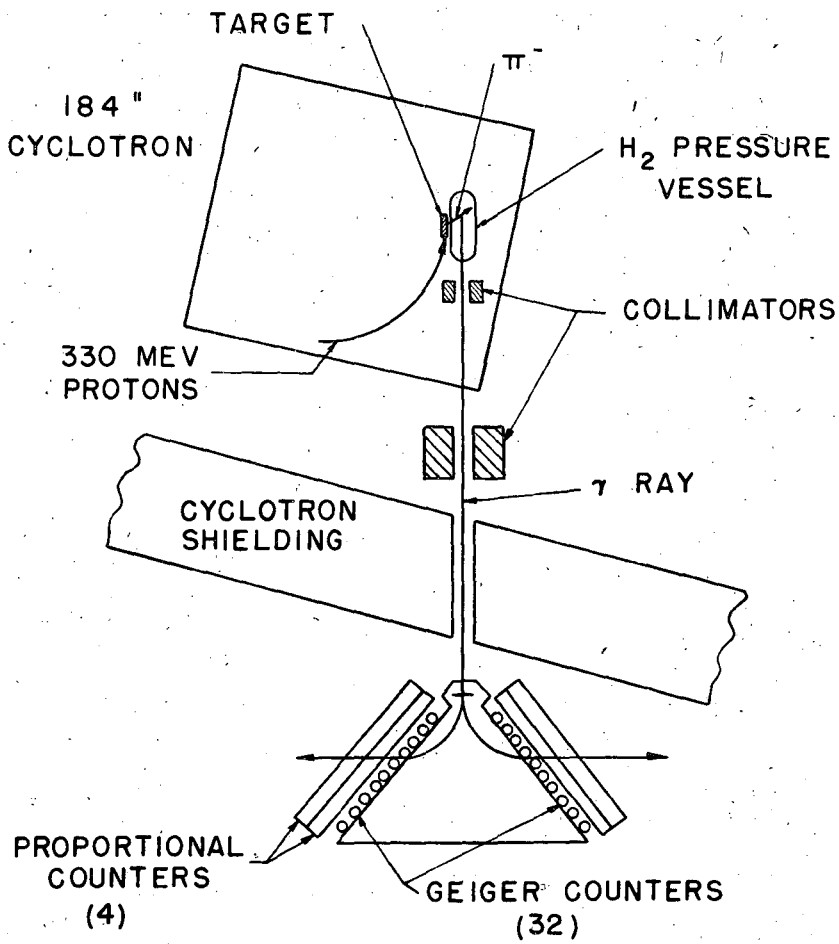
TARGET
π⁻
184"
CYCLOTRON
H2 PRESSURE
VESSEL
COLLIMATORS
330 MEV
PROTONS
γ RAY
CYCLOTRON
SHIELDING
PROPORTIONAL
COUNTERS
(4)
GEIGER COUNTERS
(32)

FIG. 1

MU 791

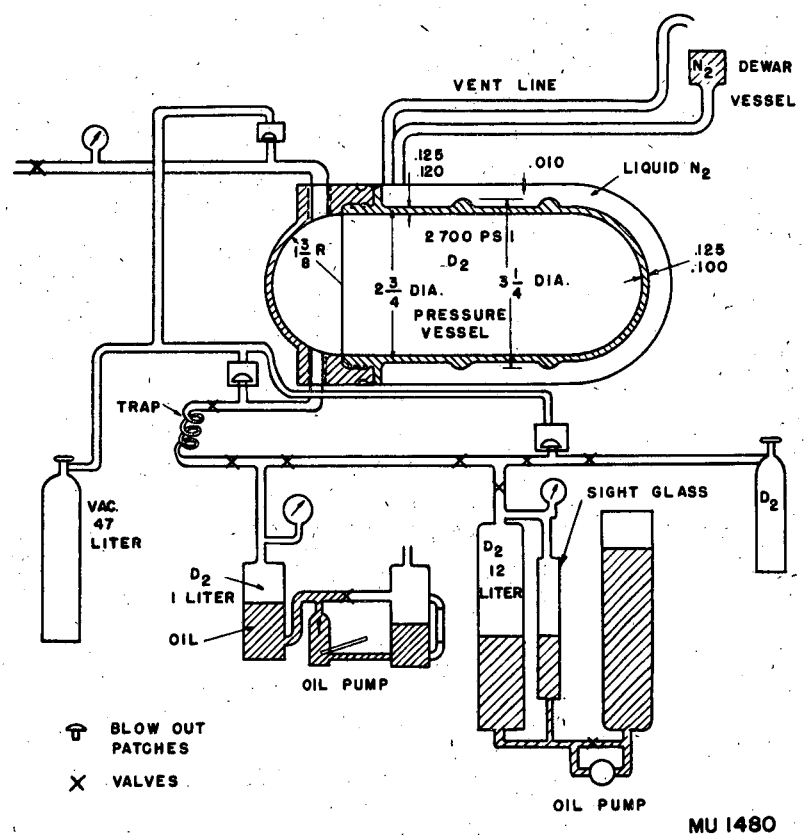
VENT LINE
N_2
DEWAR
VESSEL
.125
.120
.010
LIQUID N_2
2700 PSI
D_2
$1\frac{3}{8}$ R
$2\frac{3}{4}$ DIA.
$3\frac{1}{4}$ DIA.
.125
.100
PRESSURE
VESSEL
TRAP
VAC.
47
LITER
D_2
1 LITER
OIL
OIL PUMP
D_2
12
LITER
SIGHT GLASS
D_2
OIL PUMP
BLOW OUT
PATCHES
VALVES
MU 1480

Fig. 2

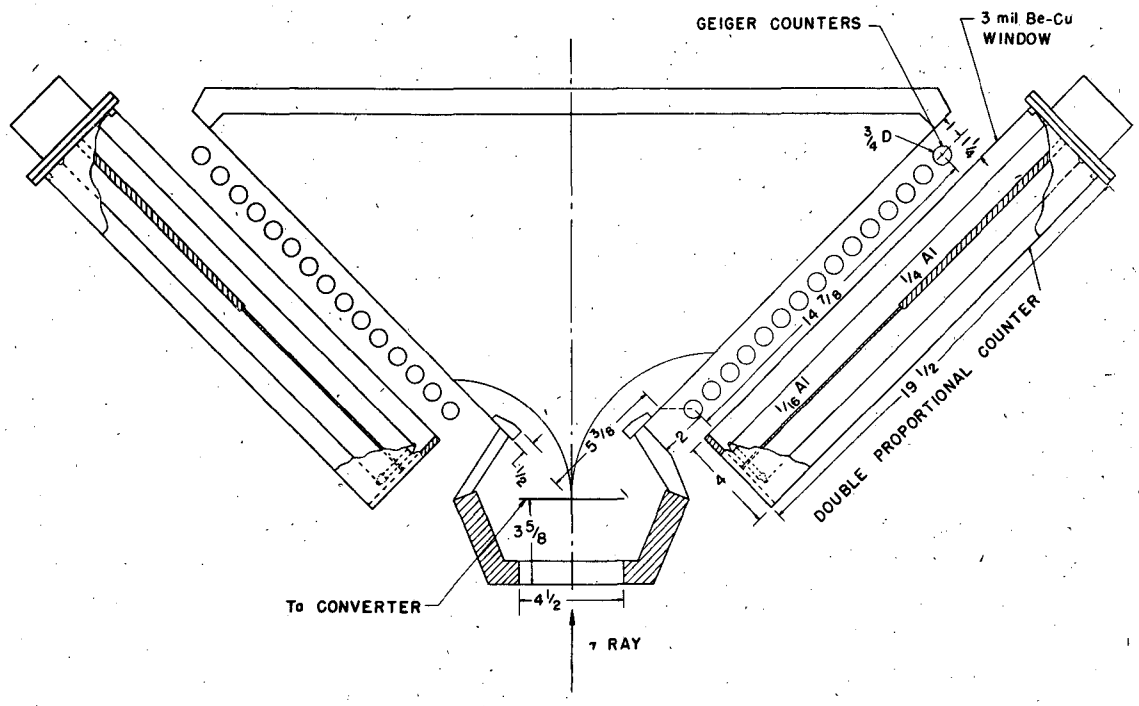
GEIGER COUNTERS
3 mil Be-Cu WINDOW
3/4 D
1 1/4
14 7/8
1/4 Al
1/16 Al
19 1/2
DOUBLE PROPORTIONAL COUNTER
2
4
5 3/8
1/2
3 5/8
4 1/2
To CONVERTER
γ RAY

MU 794

Fig. 3

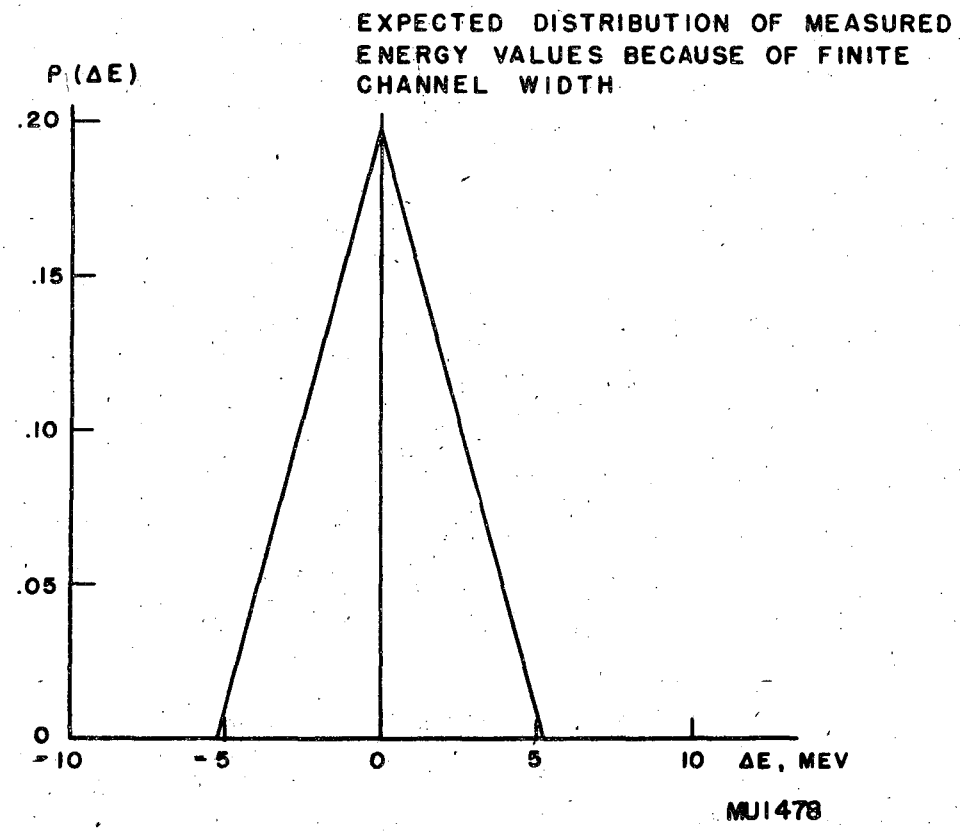
EXPECTED DISTRIBUTION OF MEASURED ENERGY VALUES BECAUSE OF FINITE CHANNEL WIDTH
P(ΔE)
.20
.15
.10
.05
0
-10
-5
0
5
10
ΔE, MEV
MU1478

Fig. 4

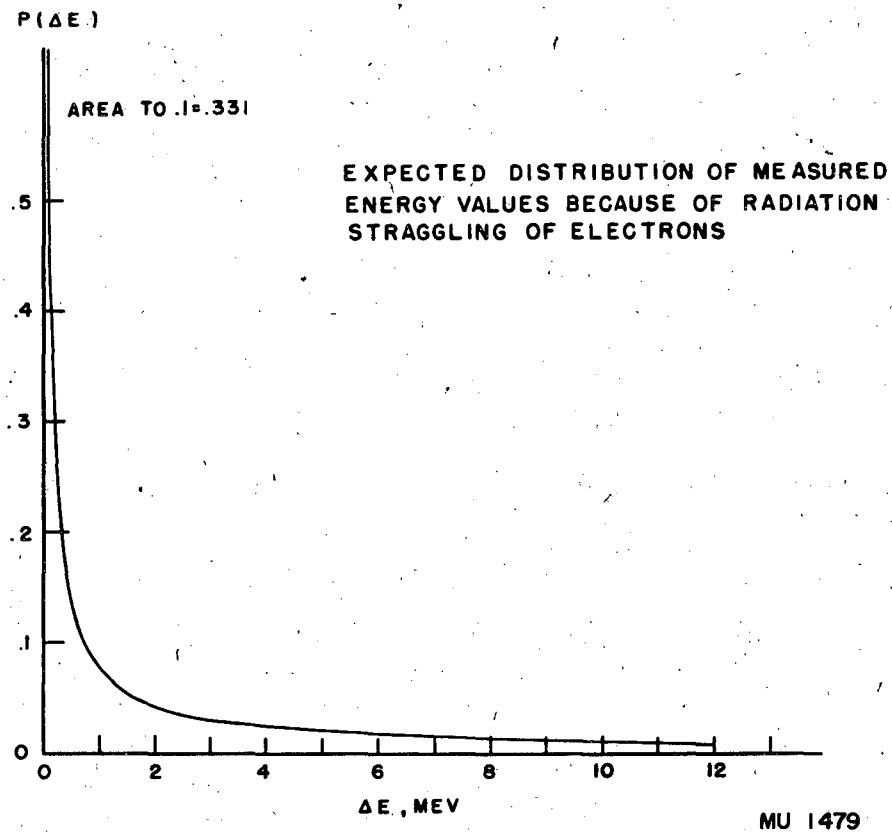
P(ΔE)
AREA TO .1=.331
EXPECTED DISTRIBUTION OF MEASURED ENERGY VALUES BECAUSE OF RADIATION STRAGGLING OF ELECTRONS
.5
.4
.3
.2
.1
0
0
2
4
6
8
10
12
ΔE, MEV
MU 1479

Fig. 5

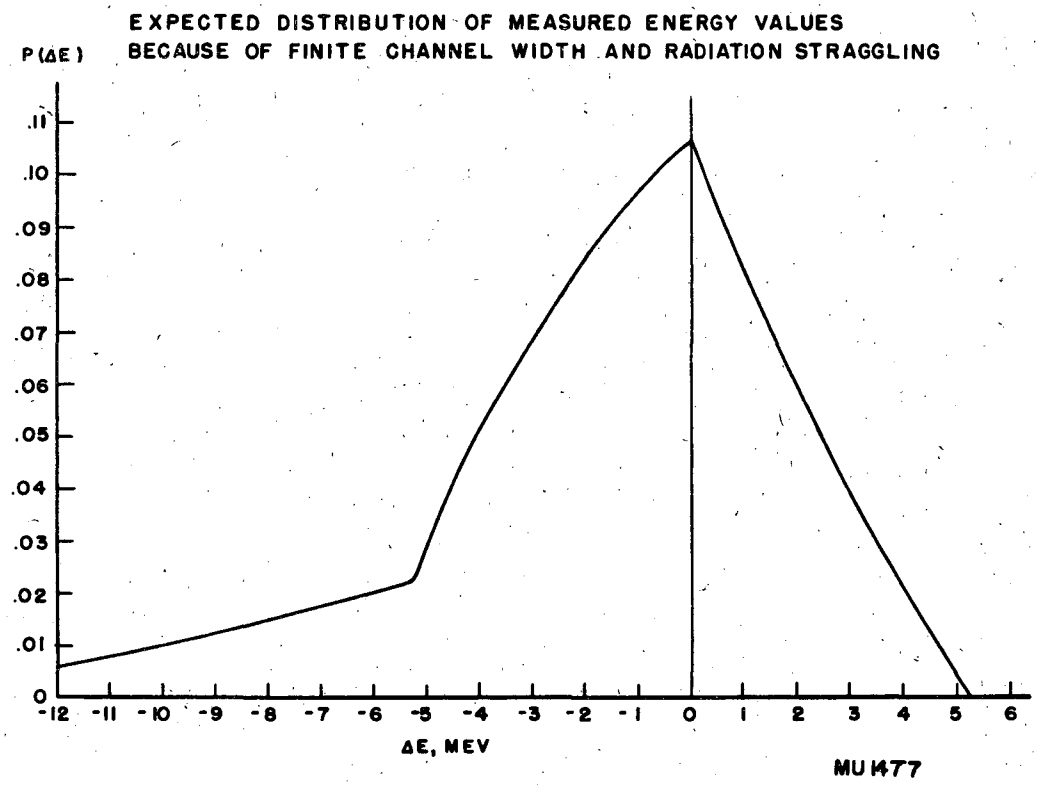
EXPECTED DISTRIBUTION OF MEASURED ENERGY VALUES
BECAUSE OF FINITE CHANNEL WIDTH AND RADIATION STRAGGLING
P(ΔE)
.11
.10
.09
.08
.07
.06
.05
.04
.03
.02
.01
0
-12 -11 -10 -9 -8 -7 -6 -5 -4 -3 -2 -1 0 1 2 3 4 5 6
ΔE, MEV
MU1477

Fig. 6

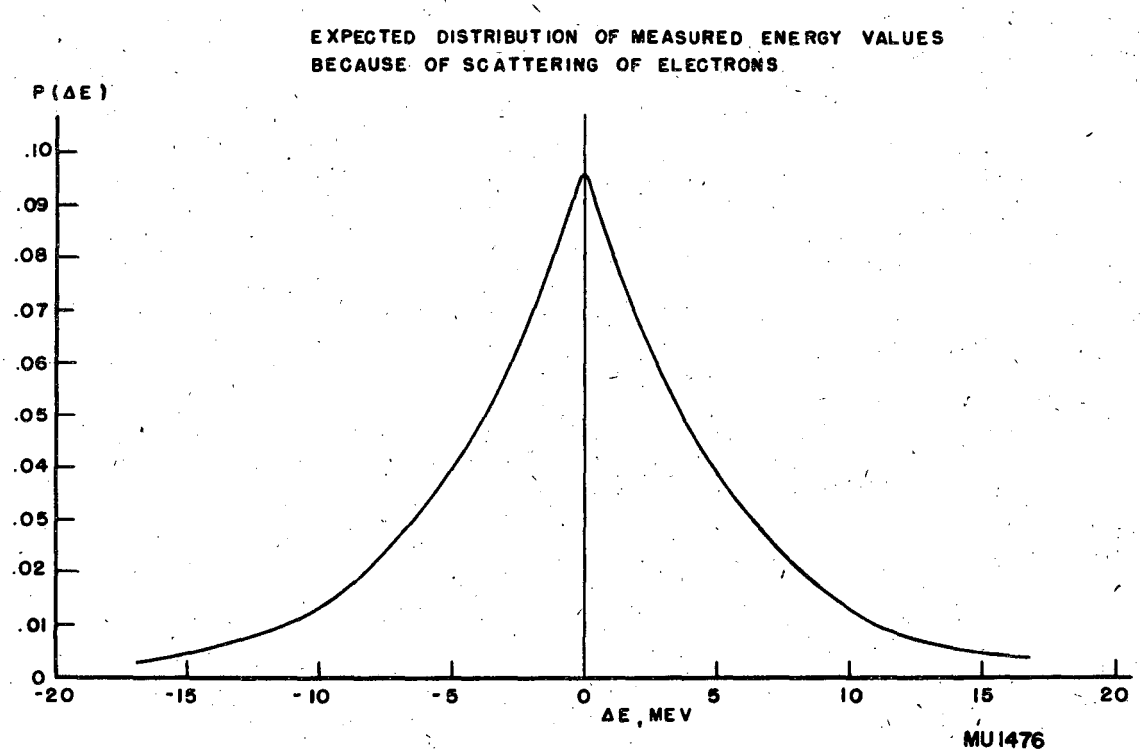
EXPECTED DISTRIBUTION OF MEASURED ENERGY VALUES
BECAUSE OF SCATTERING OF ELECTRONS
P (ΔE)
.10
.09
.08
.07
.06
.05
.04
.05
.02
.01
0
-20
-15
-10
-5
0
5
10
15
20
ΔE, MEV
MU1476

Fig. 7

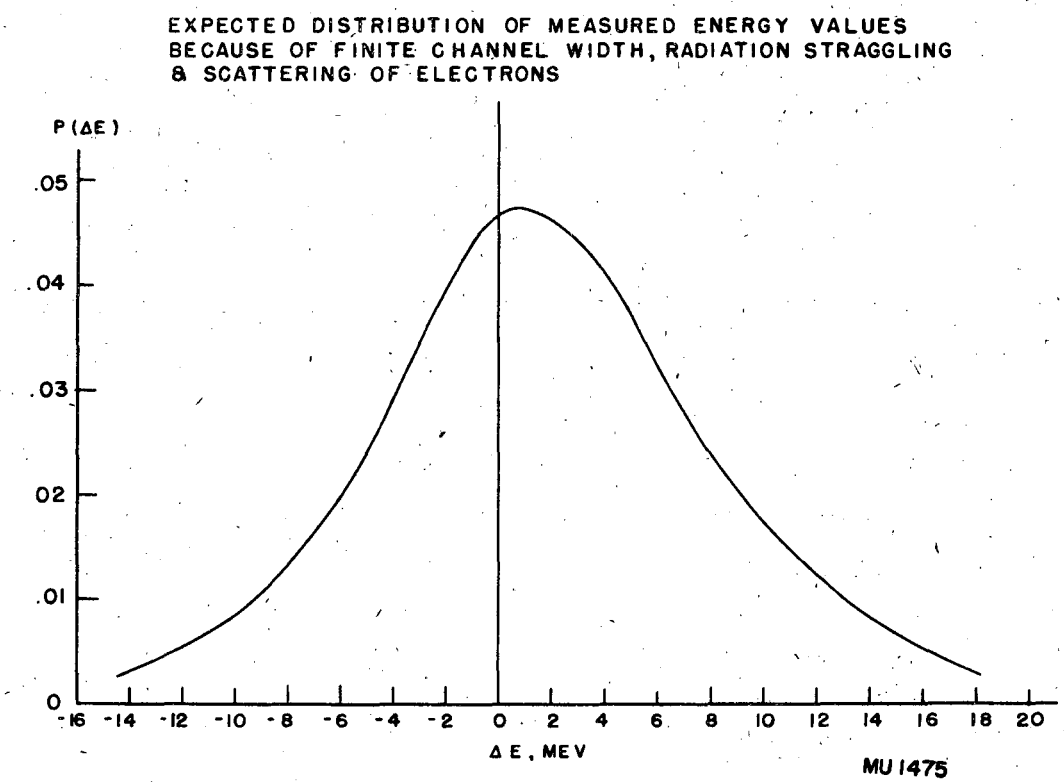
EXPECTED DISTRIBUTION OF MEASURED ENERGY VALUES
BECAUSE OF FINITE CHANNEL WIDTH, RADIATION STRAGGLING
& SCATTERING OF ELECTRONS
P (ΔE)
.05
.04
.03
02
.01
0
-16 -14 -12 -10 -8 -6 -4 -2 0 2 4 6 8 10 12 14 16 18 20
Δ E, MEV
MU 1475

Fig. 8

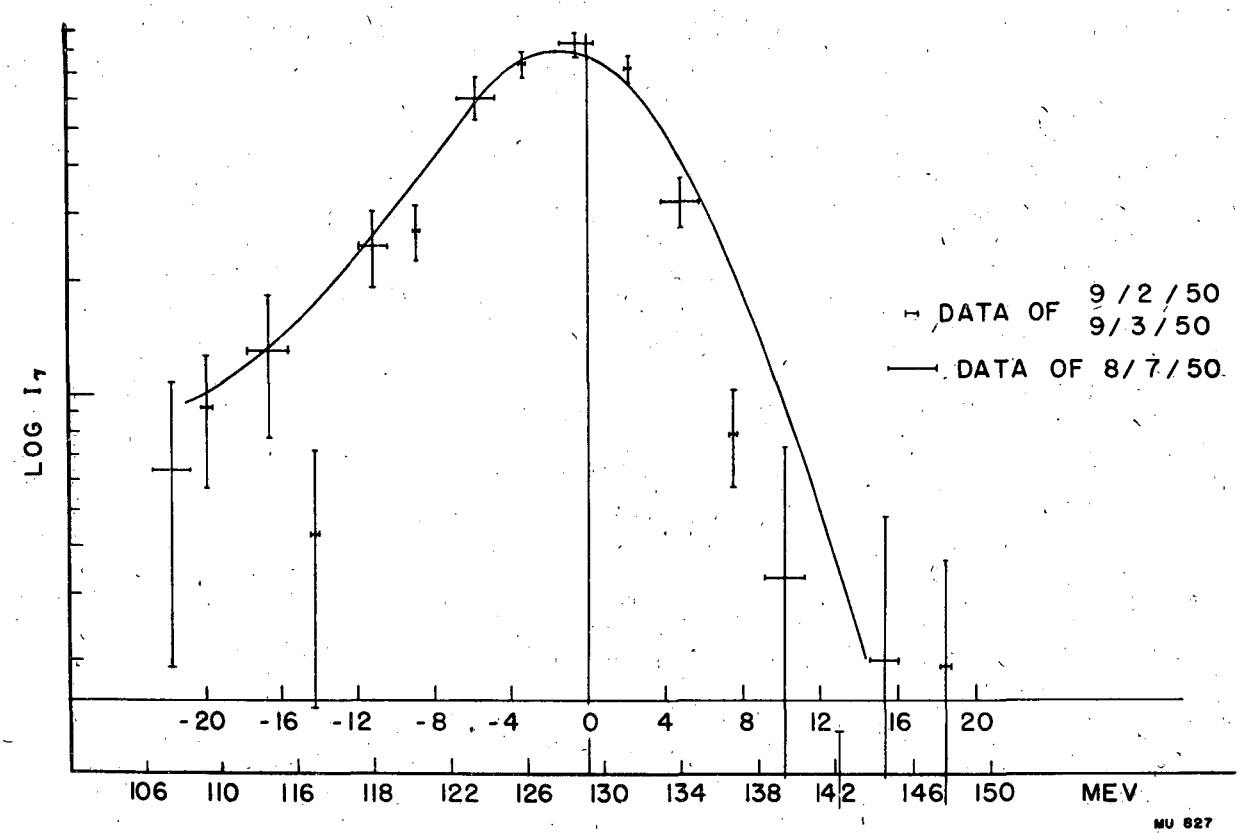
LOG I_γ
DATA OF 9/2/50 9/3/50
DATA OF 8/7/50
-20 -16 -12 -8 -4 0 4 8 12 16 20
106 110 116 118 122 126 130 134 138 142 146 150 MEV
MU 827

Fig. 9

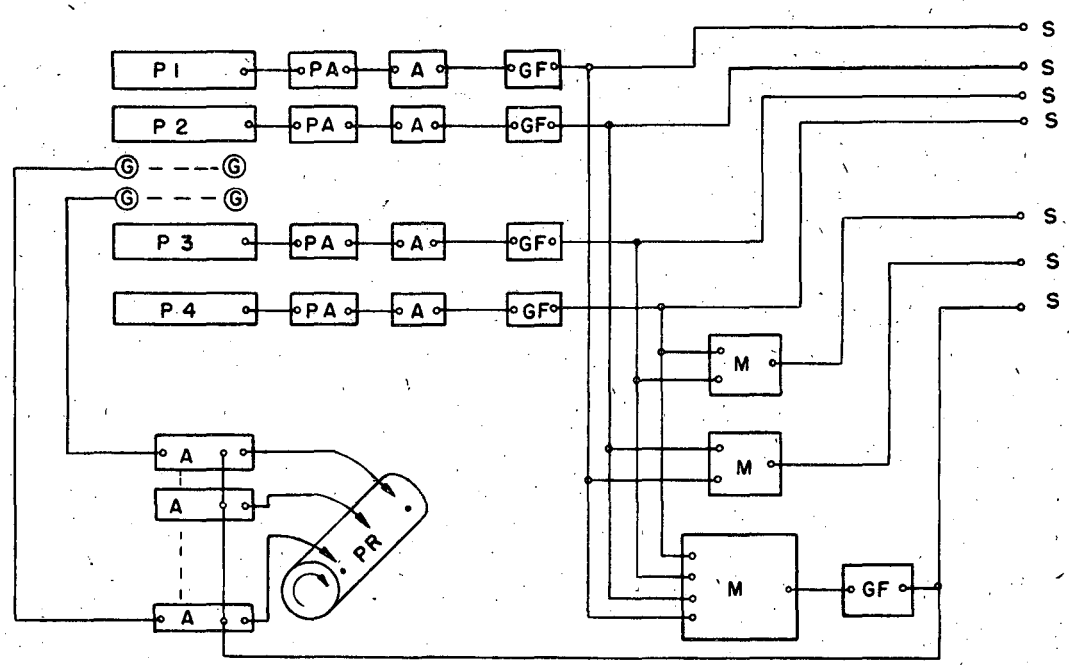

P - PROPORTIONAL COUNTER
G - GEIGER COUNTER
A - AMPLIFIER
GF - GATE FORMING UNIT
S - SCALER
PA - PRE- AMPLIFIER
M - MIXER
PR - 32 PEN RECORDER

MU 792

Fig. 10

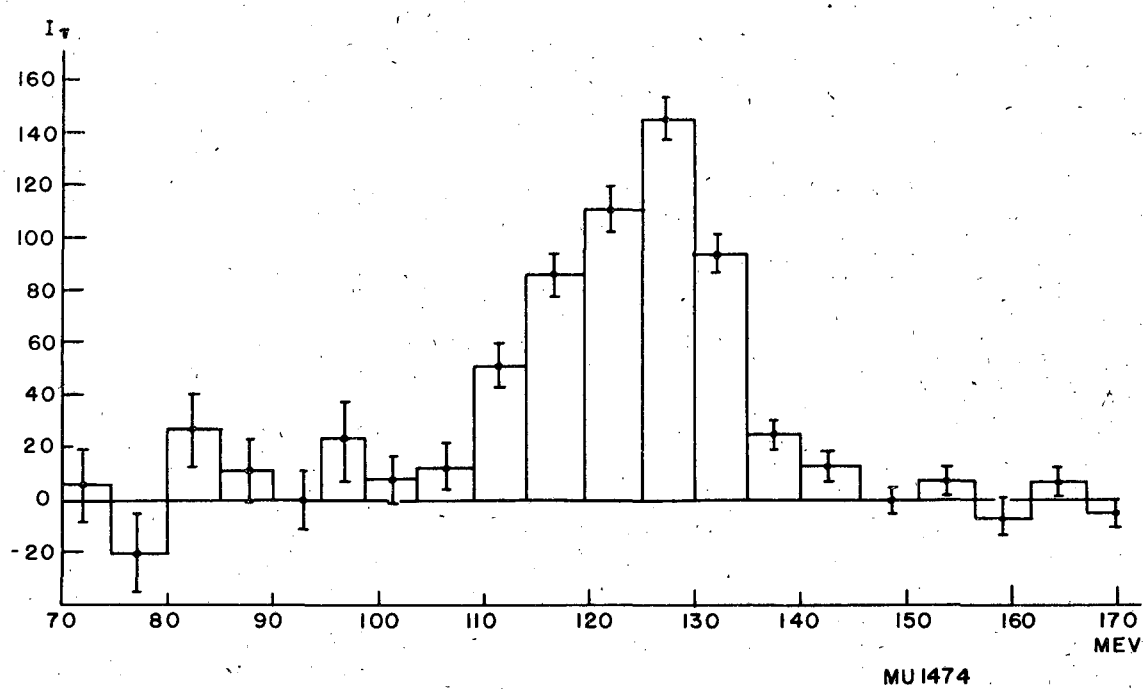
I_π
160
140
120
100
80
60
40
20
0
-20
70
80
90
100
110
120
130
140
150
160
170
MEV
MU 1474

Fig. 11

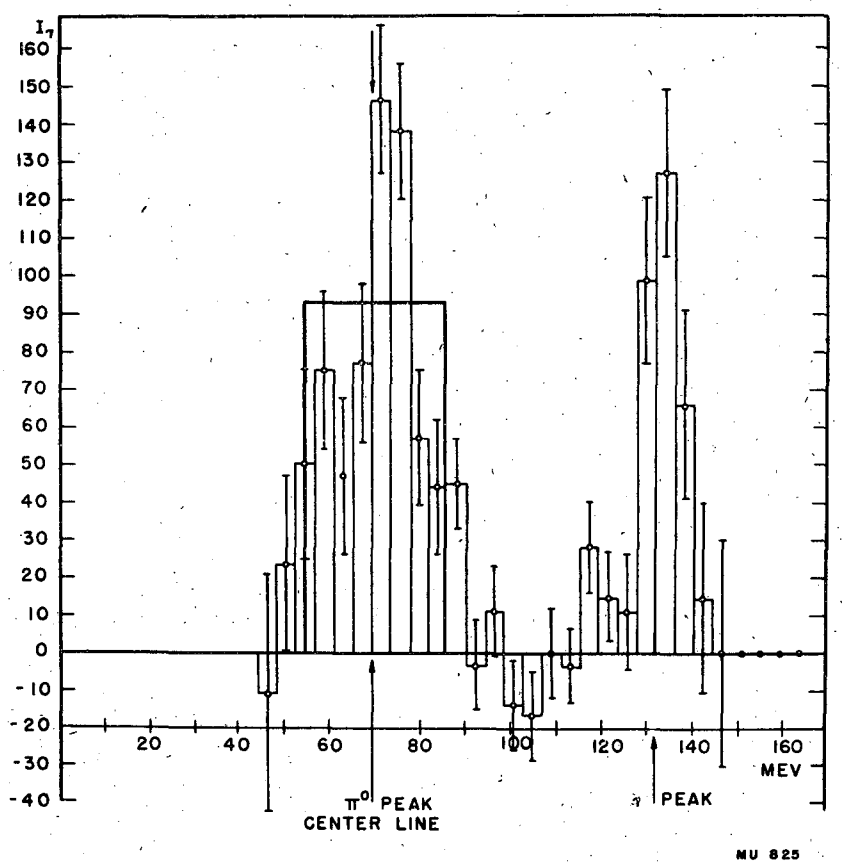
I_γ
160
150
140
130
120
110
100
90
80
70
60
50
40
30
20
10
0
-10
-20
-30
-40
20
40
60
80
100
120
140
160
MEV
π^0 PEAK
CENTER LINE
η PEAK
MU 825

Fig. 12

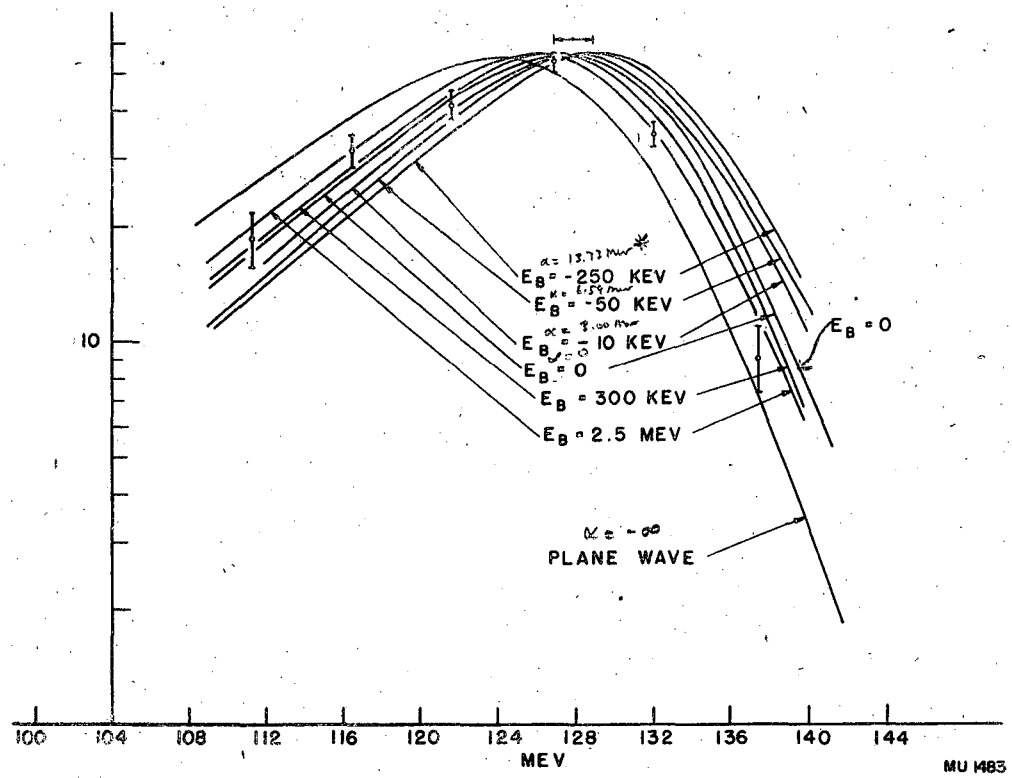

* See UCRL-1086 Fig III Fig IV

Fig. 13

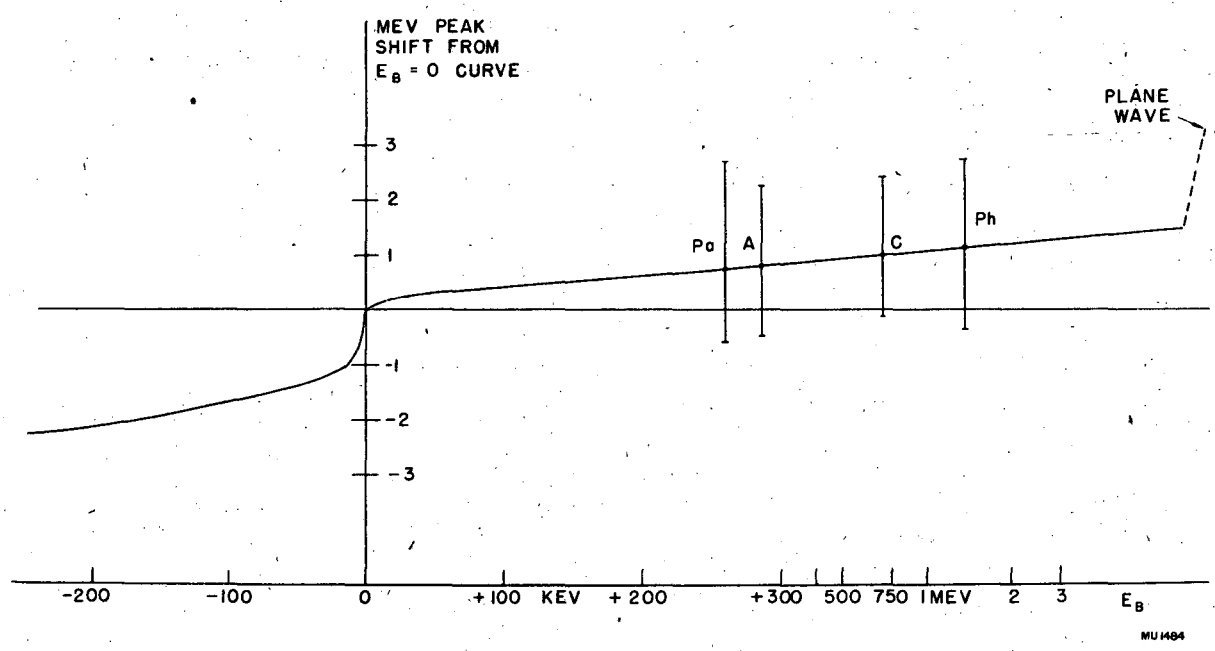
MEV PEAK
SHIFT FROM
E_B = 0 CURVE
PLANE
WAVE
3
2
1
-1
-2
-3
Pa
A
C
Ph
-200
-100
0
+100 KEV
+200
+300
500
750
1MEV
2
3
E_B
MU1484

Fig. 14

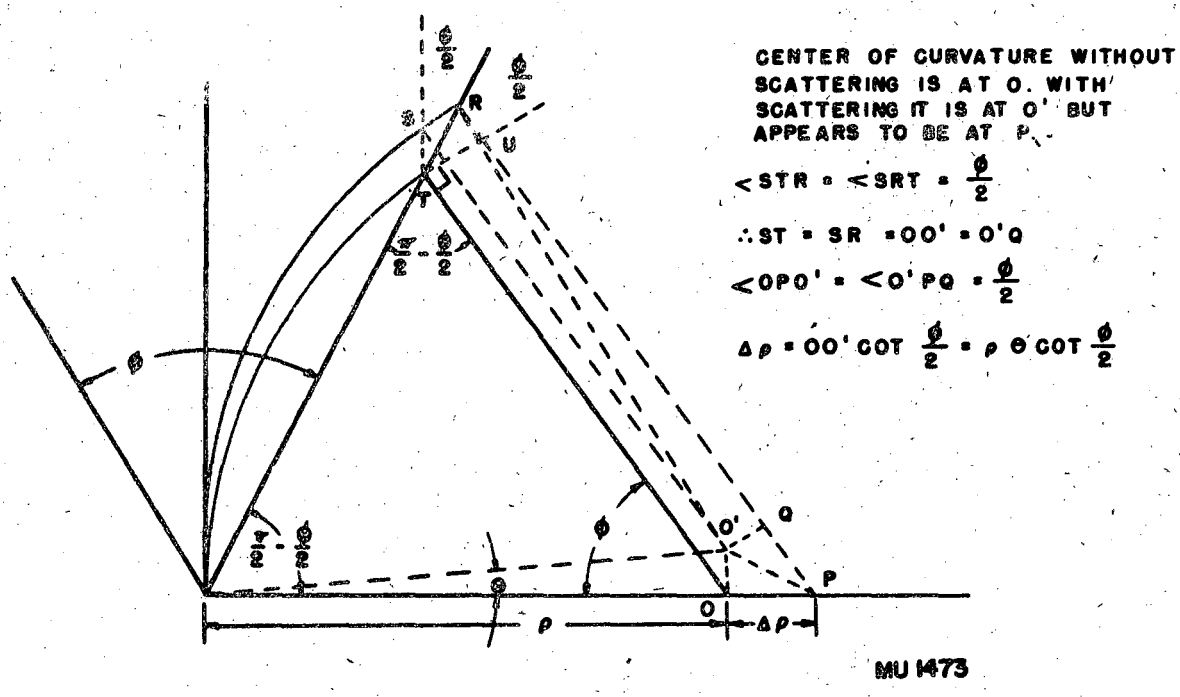
CENTER OF CURVATURE WITHOUT SCATTERING IS AT O. WITH SCATTERING IT IS AT O' BUT APPEARS TO BE AT P.
$\angle STR = \angle SRT = \frac{\phi}{2}$
$\therefore ST = SR = OO' = O'Q$
$\angle OPO' = \angle O'PQ = \frac{\phi}{2}$
$\Delta\rho = OO' \cot\frac{\phi}{2} = \rho\,\theta \cot\frac{\phi}{2}$
S
R
U
T
O'
Q
P
O
ρ
$\Delta\rho$
ϕ
MU 1473

Fig. 15

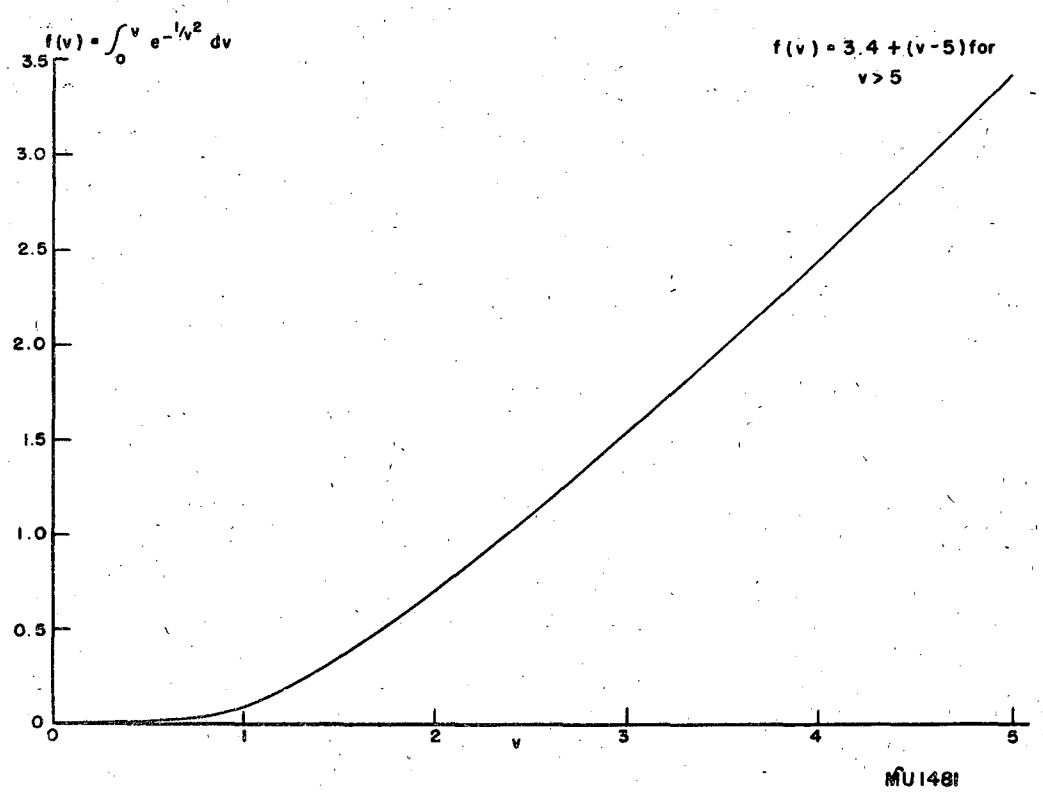

Fig. 16

UNIVERSAL SCATTERING CURVE P(x). SEE APP. B FOR EXPLANATION

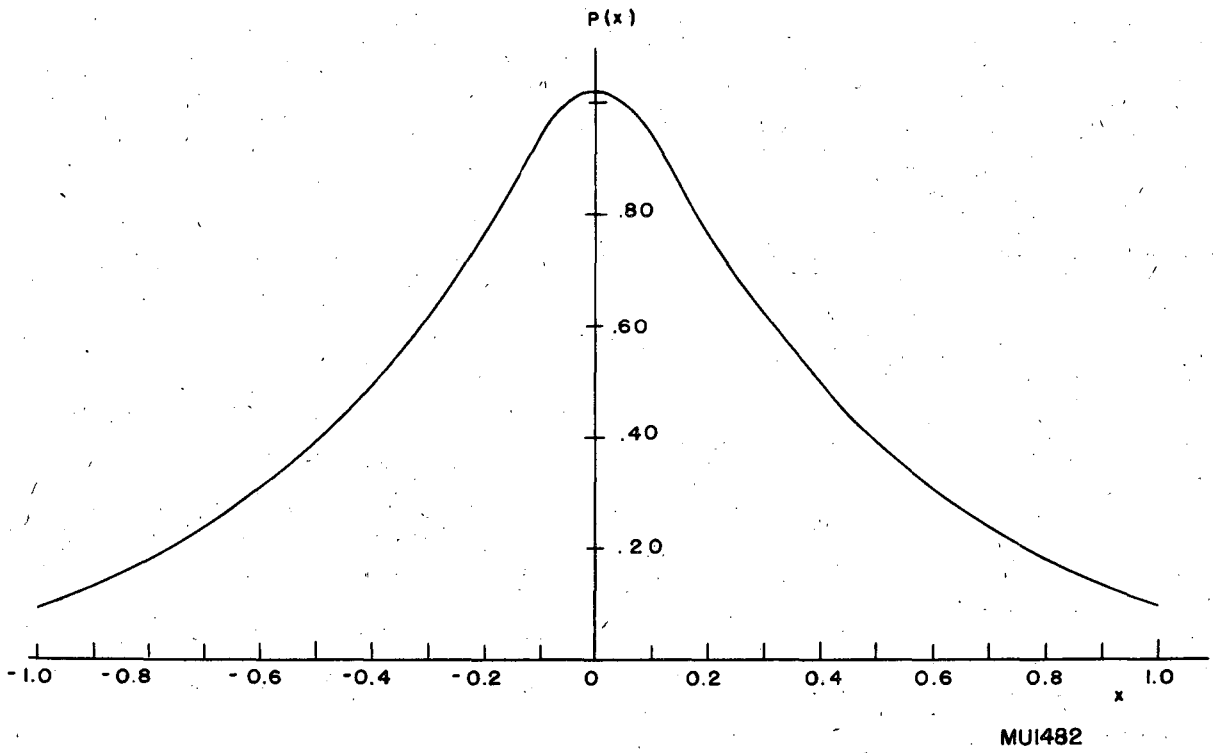

Fig. 17

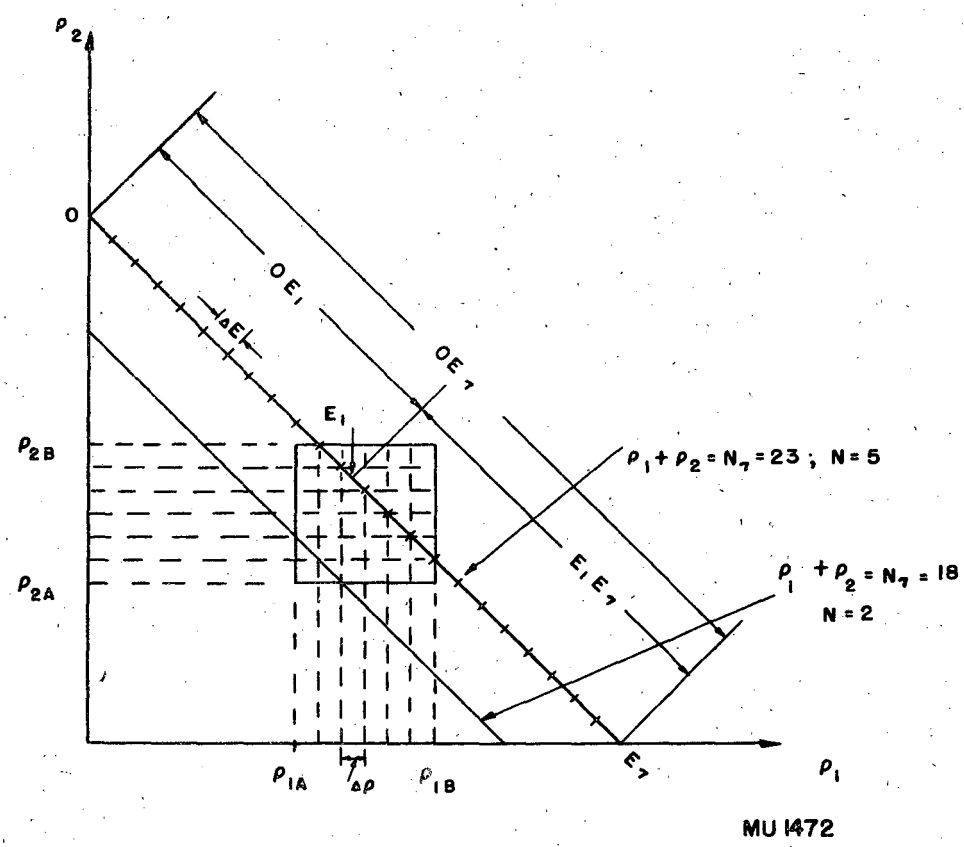
ρ_2
O
OE_1
ΔE
OE_7
E_1
ρ_{2B}
ρ_{2A}
$\rho_1 + \rho_2 = N_7 = 23$; N = 5
E_1E_7
$\rho_1 + \rho_2 = N_7 = 18$
N = 2
ρ_{1A}
$\Delta\rho$
ρ_{1B}
E_7
ρ_1
MU 1472

Fig. 18

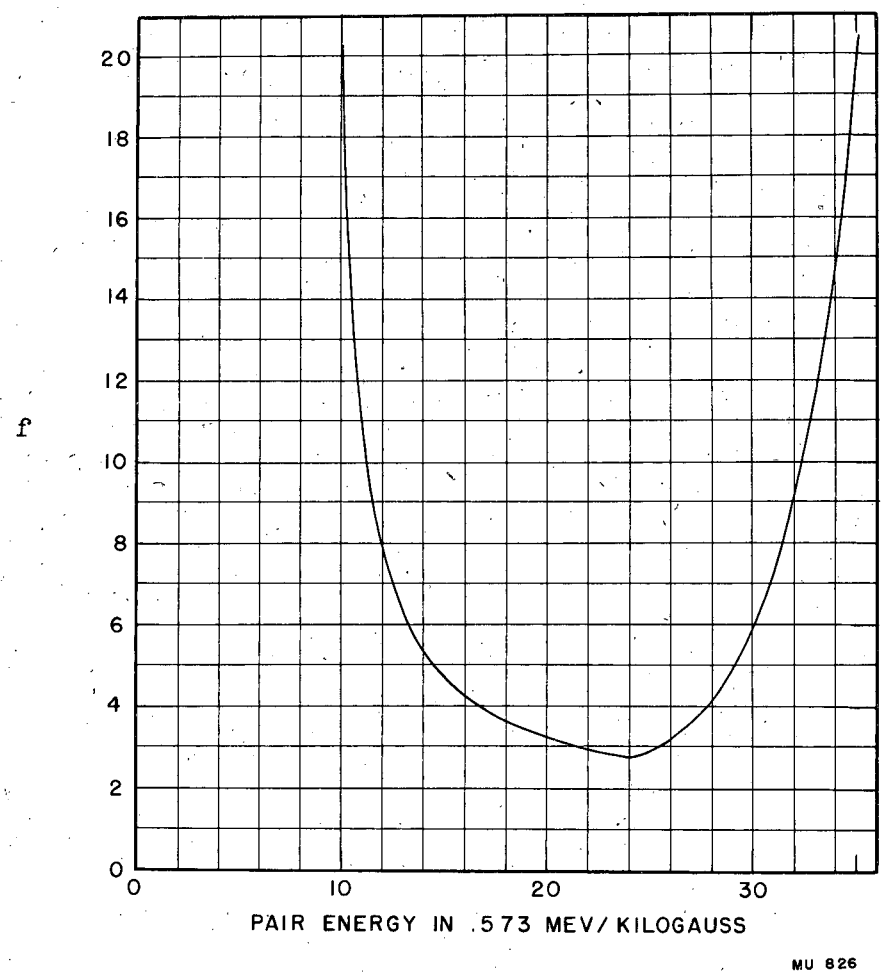
f
20
18
16
14
12
10
8
6
4
2
0
0
10
20
30
PAIR ENERGY IN .573 MEV/KILOGAUSS
MU 826

Fig. 19

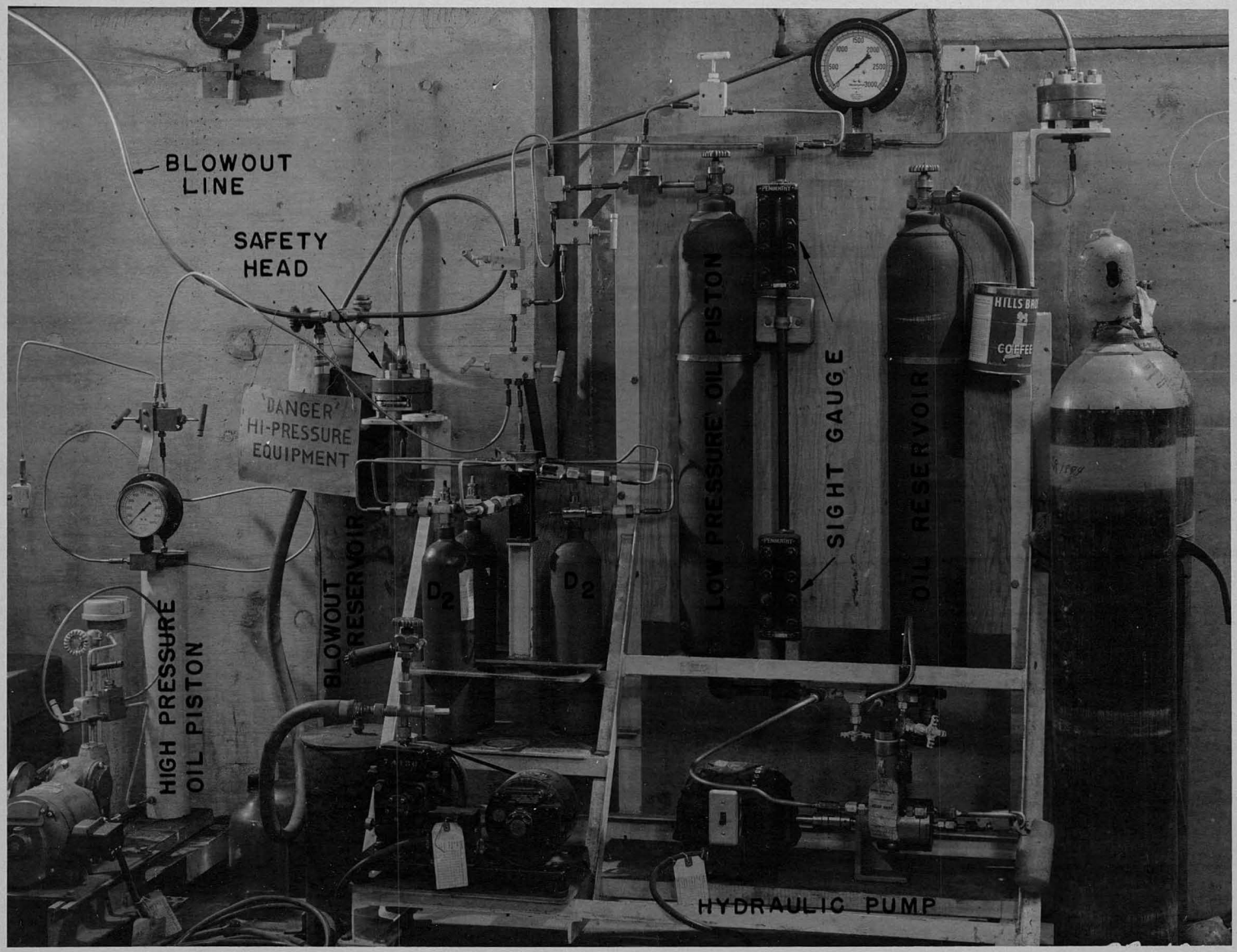

FIG. 20

OZ 1226